# Toward N-Doped Graphene via Solvothermal Synthesis

Dehui Deng,[†] Xiulian Pan,*[,†] Liang Yu,[†] Yi Cui,[†] Yeping Jiang,[‡] Jing Qi,[§] Wei-Xue Li,[†] Qiang Fu,[†] Xucun Ma,[‡] Qikun Xue,[‡] Gongquan Sun,[§] and Xinhe Bao*[,†]

[†]State Key Laboratory of Catalysis, Dalian Institute of Chemical Physics, The Chinese Academy of Sciences, Zhongshan Road 457, Dalian 116023, China

[‡]Institute of Physics, The Chinese Academy of Sciences, Beijing 100190, China

[§]Direct Alcohol Fuel Cell Laboratory, Dalian Institute of Chemical Physics, Chinese Academy of Science, Zhongshan Road 457, Dalian 116023, China

Ⓢ Supporting Information

ABSTRACT: Theoretical studies predicted that doping graphene with nitrogen can tailor its electronic properties and chemical reactivity. However, experimental investigations are still limited because of the lack of synthesis techniques that can deliver a reasonable quantity. We develop here a novel method for one-pot direct synthesis of N-doped graphene via the reaction of tetrachloromethane with lithium nitride under mild conditions, which renders fabrication in gram scale. The distinct electronic structure perturbation induced by the incorporation of nitrogen in the graphene network is observed for the first time by scanning tunnelling microscopy. The nitrogen content varies in the range of 4.5–16.4%, which allows further modulation of the properties. The enhanced catalytic activity is demonstrated in a fuel cell cathode oxygen reduction reaction with respect to pure graphene and commercial carbon black XC-72. The resulting N-doped materials are expected to broaden the already widely explored potential applications for graphene.

KEYWORDS: graphene, N-doped, solvothermal, electrocatalysis, oxygen reduction reaction
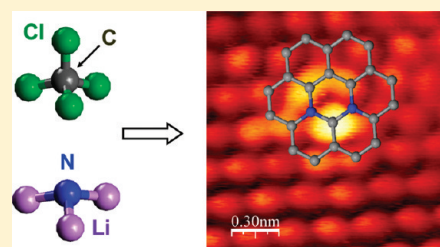
■ INTRODUCTION

Graphene has stimulated wide interest because of the properties associated with the two-dimensional (2-D) crystal structure formed by sp^2 hybridized carbon. Extensive studies have shown great promise for applications in fields such as electronics, sensors, batteries, supercapacitors, and catalysts.[1−4] Theoretical studies revealed that doping graphene with nitrogen is effective to tailor its electronic property and chemical reactivity[5−7] because of the stronger electronegativity of nitrogen compared to that of carbon and conjugation between the nitrogen lone pair electrons and the graphene π-system. This could create novel nanomaterials and expand its already widely explored potential applications. However, there are only a handful of studies on preparation of N-doped graphene so far. For example, treating preformed graphene or graphite oxide in ammonia at high temperatures[8] or using ammonia plasma[9] were effective to introduce N into graphene. N-doped graphene was grown on a Cu film/Si single crystal substrate by chemical vapor deposition at 800 °C.[10] Arc discharge of graphite electrodes in the presence of H₂, He, and pyridine vapor was developed recently.[11] However, future applications rely on easy-to-operate methods, which can deliver products in a reasonably large quantity.

Solvothermal processes are known for the simple operation, mild synthesis conditions, and capability to deliver relatively large quantities. Several processes have been developed previously for nanostructured carbon materials. For example, diamond was synthesized via the reaction of tetrachloromethane and sodium[12] and carbon nanotubes (CNTs) from the reaction of hexachlorobenzene with metallic potassium catalyzed by Co/Ni.[13] The reaction of hexachlorobenzene and sodium led to the formation of carbon nanospheres.[14] More recently, a gram-scale pure graphene was obtained via the reaction of ethanol and sodium.[15] We demonstrate here a new solvothermal process for synthesis of N-doped graphene based on the reaction of tetrachloromethane with lithium nitride below 350 °C. To the best of our knowledge, this is the first study on a one-step direct chemical synthesis of this material. We believe that this facile method will enable production of N-doped graphene at a larger scale because the yield is only limited by the capacity of the autoclave. With a 40 mL autoclave, we obtained about 1.2 g of product per batch (Figure 1a).
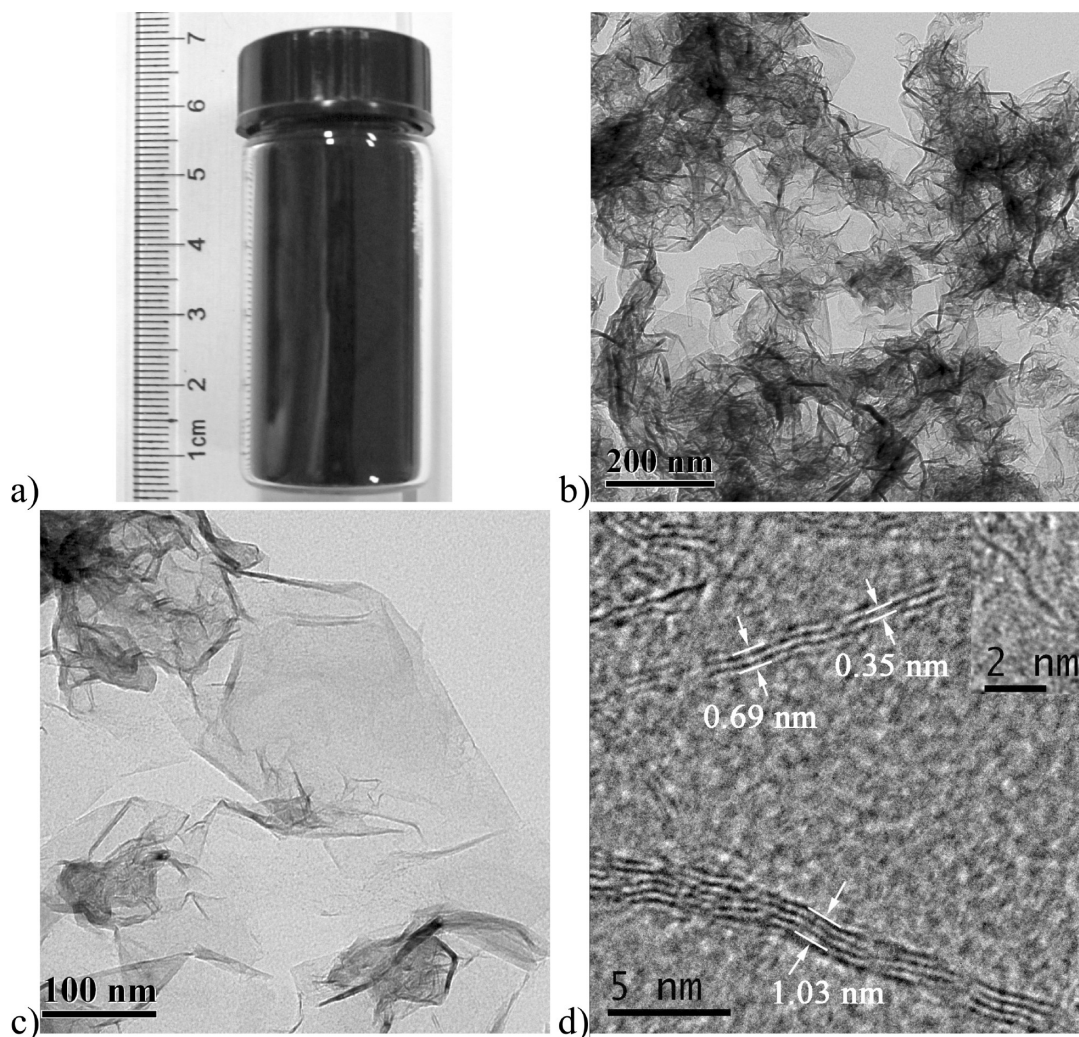
■ EXPERIMENTAL SECTION

NG-1 Synthesis. The reaction of lithium nitride (1 g) and tetrachloromethane (20 mL) was carried out at 250 °C for 10 h in a 40 mL stainless steel autoclave in nitrogen. The product was washed sequentially with 18 wt % HCl aqueous solution, water, and ethanol, followed by drying at 120 °C for 12 h.

Figure 1. (a) Vial containing NG-1 (1.2 g) obtained with a 40 mL autoclave per batch in the laboratory. (b,c) TEM images of NG-2 at different magnifications. (d) HRTEM images of NG-1 showing the cross sections of single (inserted image) to four layer graphene.

NG-2 Synthesis. Cyanuric chloride (0.5 g) was mixed with lithium nitride (2 g) and tetrachloromethane (5 mL), and the reaction was carried out at 350 °C for 6 h. The product was washed and dried following the same procedure as NG-1. All chemicals were purchased from Alfa Aesar.

Characterization and Theoretical Simulation. STM analysis was conducted in a Unisoku UHV low-temperature STM system equipped with a molecular beam epitaxy chamber. The base pressure is 5.0×10^{-11} Torr. N-doped graphene was dispersed in ethanol and dipped on a SiC (0001) crystal substrate. The SiC substrate was covered in advance by epitaxially grown graphene.[16] XPS analysis was conducted with an Omicron UHV multiprobe surface analysis system (2.0×10^{-10} Torr). The sample was supported on a Ag substrate. TEM was carried out on a FEI Tecnai F30 microscope and a G^2 microscope operated at an accelerating voltage of 300 and 120 kV, respectively. The samples were placed onto an ultrathin carbon film supported on a copper grid. Raman spectroscopy was performed on a Jobin Yvon LabRAM HR 800 instrument with a 633 nm excitation laser at a power of around 0.8 mW. The electrical resistivities of the samples were measured using a four-probe method (SZ-82, four-probe measure apparatus, Suzhou, China). The preliminary measurement indicated that the electrical conductivities of NG-1 (resistivity 0.18 Ω cm) and NG-2 (0.15 Ω cm) were comparable to that of XC-72 (0.08 Ω cm) but better than a commercial carbon black (Alfa Aesar) (1.00 Ω cm). The STM topological images were simulated using DFT, adopting Tersoff and Hamann approximation[17] in a constant height mode. A model of bilayer graphene with the Bernal (i.e., AB) stacking was used in the simulation, and the distance between the layers was 0.34 nm. The calculation was carried out at the experimental bias voltage (0.9 V). The electron density of both layers in the range of 0−0.90 eV above the Fermi level is integrated for the images.

RESULTS AND DISCUSSION

The sample synthesized from the reaction of lithium nitride with tetrachloromethane was named as NG-1 here. Nitrogen-containing precursors can be added during synthesis to increase the nitrogen content. For example, NG-2 was obtained with the aid of cyanuric chloride. Panels b−c of Figure 1 and Figure S1 of the Supporting Information display transmission electron microscopy (TEM) images of NG-1 and NG-2 at different magnifications. They exhibit the typical nanosheet structure of graphene. High resolution TEM (HRTEM) characterization indicates further that these nanosheets mainly consist of 1−6 layers, and Figure 1d shows the cross sections of 1−4 layer graphene. The interlayer distance is 0.35 ± 0.01 nm, in agreement with the interlayer distance of graphite.

X-ray photoelectron spectroscopy (XPS) is a proficient and commonly used technique to examine the features of nitrogen
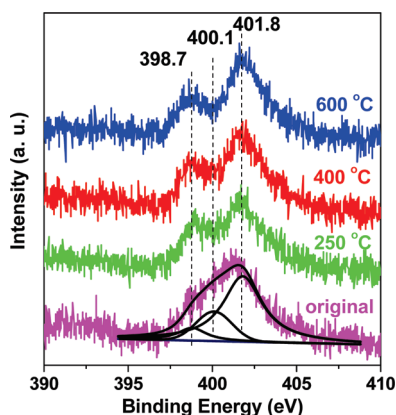
Figure 2. N1s XPS spectra of NG-1 upon in situ heat treatment. Fitting this signal indicates the presence of graphitic (401.8 eV), pyridinic (398.7 eV), and pyrrolic (400.1 eV) nitrogen species.

species in carbon materials such as graphite and CNTs.[18,19] The spectra in Figure 2 and Figure S2 of the Supporting Information demonstrate that nitrogen species have been successfully incorporated into both NG-1 and NG-2. Apart from carbon, nitrogen, oxygen, and chlorine, no other elements are observed. The atomic ratio of N/C can be estimated from the peak areas of C 1s and N 1s and their atomic sensitivity factors and is often used to describe the nitrogen content.[19] As listed in Table S1 of the Supporting Information, this ratio is 4.5% for NG-1. Fitting the N 1s signal (Figure 2) indicates the presence of three types of species, pyridinic N (398.7 eV), pyrrolic N (400.1 eV), and graphitic N (401.8 eV), consistent with the results for other N-doped carbon materials.[10,20] As depicted by the model in Figure S3 of the Supporting Information, pyridinic N bonds with two C atoms with one p-electron localized in the π conjugated system and pyrrolic N with two p-electrons, respectively. Graphitic N substitutes a C atom in the hexagonal ring, which dominates in NG-1. In comparison, the N/C ratio reaches 16.4% in NG-2, which is more than 3 times higher than that in NG-1 and also higher than the content of 2−10% often reported for N-doped CNTs.[18,21] The same three types of N species are observed (Figure S2b of the Supporting Information), but pyridinic and pyrrolic N dominate in NG-2.

The stability of the nitrogen species in the graphene structure was examined by in situ heat treatment in the ultrahigh vacuum (UHV) chamber of the XPS instrument. Figure 2 and Tables S1−S2 of the Supporting Information show that the N/C ratio decreases, for example, from 4.5% to 3.0% for NG-1 treated at 600 °C and from 16.4 to 10.5% for NG-2 treated at 600 °C. The amount of pyrrolic N drops most significantly, while those of graphitic and pyridinic N species decrease only slightly. It indicates that the latter two N species are rather thermally stable compared to pyrrolic N in the graphene structure.

Further insights of the structural and electronic properties of graphene are obtained from Raman spectroscopy characterization. We carried out measurements on the powdered samples, which can provide the global information of graphene in contrast to TEM characterization of much smaller sections of the sample. As displayed in Figure 3a, the characteristic D and G bands of carbon materials are observed at around 1350 and 1585 cm^{-1}, respectively.[22,23] The D band is associated with disordered samples or graphene edges, while the G band is the result of the first-order scattering of the E_{2g} mode of sp^2 carbon domains.

Both bands can be influenced by doping. For example, D bands are significantly enhanced in NG-1 and NG-2 with respect to pure graphene[24] because pyridinic and pyrrolic N are accompanied by defects inside the graphene network and functional edges of graphene sheets.[10,25] Furthermore, the G bands split into two peaks upon N-doping (Figure 3b), which was also observed in N-doped graphene derived from ammonia plasma treatment of pure graphene.[9] It is interesting to note that the G band of NG-1 shifts to lower frequency by 4 cm^{-1}, whereas that of NG-2 moves to higher frequency by 3 cm^{-1} with respect to that of pure graphene (Figure 3b), implying that there might be different types of dopants in NG-1 and NG-2. Previous theoretical simulations on N-doped CNTs suggest that substitution of C atoms with graphitic N was n-type doping, while pyridinic and pyrrolic N was p-type doping.[26−28] Because NG-1 contains more graphitic N while NG-2 has more pyridinic and pyrrolic N, G band shifts in NG-1 and NG-2 agree with the earlier observation of downshift in n-type and upshift in p-type doped graphite and CNTs.[29,30] Another characteristic feature of graphene is the second-order two phonon mode G′ band near 2660 cm^{-1}, which are slightly broadened but remain symmetric in NG-1 and NG-2,[22,31] in contrast to a split peak for multilayer graphene,[23,32] bulk graphite[24], and severely broadened peak for XC-72.

The structure of the N-doped graphene is further examined by low-temperature scanning tunneling microscopy (LT-STM, −196 °C) at the atomic scale. Although STM simulation of N-doped graphene has just recently been reported,[33] experimental studies have not been carried out yet. We dispersed the sample on an epitaxial graphene supported by a SiC (0001) single crystal substrate and transferred it into the UHV chamber (5.0 × 10^{-11} Torr). The sample was annealed at 500 °C prior to STM observation. Figure 4a shows a typical isolated bilayer graphene with a height of about 0.8 nm thick, as depicted by the inserted dark line profile. For comparison, the STM image of the substrate is displayed in Figure S4 of the Supporting Information, which shows a perfect monolayer graphene with a well-defined honeycomb structure.[34] The STM images in panels b and c of Figure 4 show the fine triangular grid structure of this bilayer with a lattice constant of 2.4 ± 0.1 Å, in agreement with a pure graphene bilayer with the Bernal (i.e., AB) stacking.[34,35] More importantly, sections brighter than the main graphene network are observed in STM images, indicating the presence of defects, which perturb the electronic structure of graphene. The sizes of these bright areas are smaller than 0.5 nm. Earlier experimental and theoretical studies had revealed that defects caused by a missing C atom or the oxygen-containing groups in graphene were usually larger than 1 nm because of the scattering effects in STM measurements.[36−39] Therefore, this perturbed structure is likely due to the doped N atoms. To gain further insight into the doping effect on the structure of graphene, we carried out density functional theory (DFT) calculations. We find that these bright spots are not the images of N atoms, in agreement with an earlier STM simulation.[33] Moreover, the adjacent C atoms exhibit a higher brightness because of the increased electron density of states near the Fermi level brought by the doped N atoms. Panel d in Figure 4 is a simulated STM based on the Tersoff and Hamann theory, which contains two N atoms at the meta positions (denoted by deep blue balls) in one benzene ring (represented by gray balls). The simulated STM agrees rather well the measured structure in panel c of Figure 4. Therefore, the perturbed electronic structure is most likely caused by the incorporation of nitrogen in the graphene network.
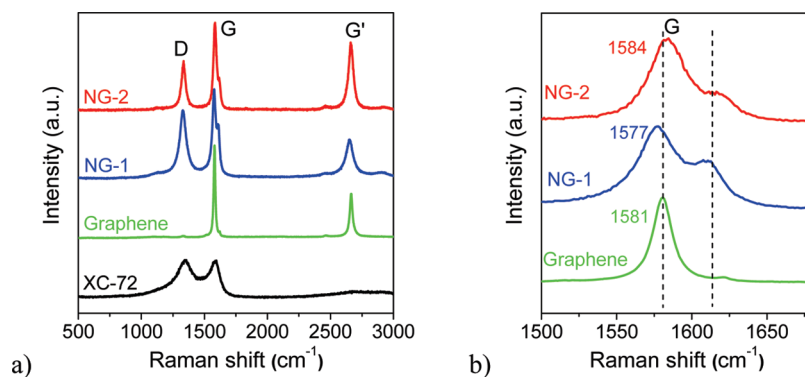
Figure 3. (a) Raman spectra of NG-1 and NG-2 in comparison to those of pure graphene and commercial carbon black XC-72. (b) G bands of NG-1 and NG-2 in comparison to that of pure graphene (obtained by thermal splitting of SiC granules[24]).
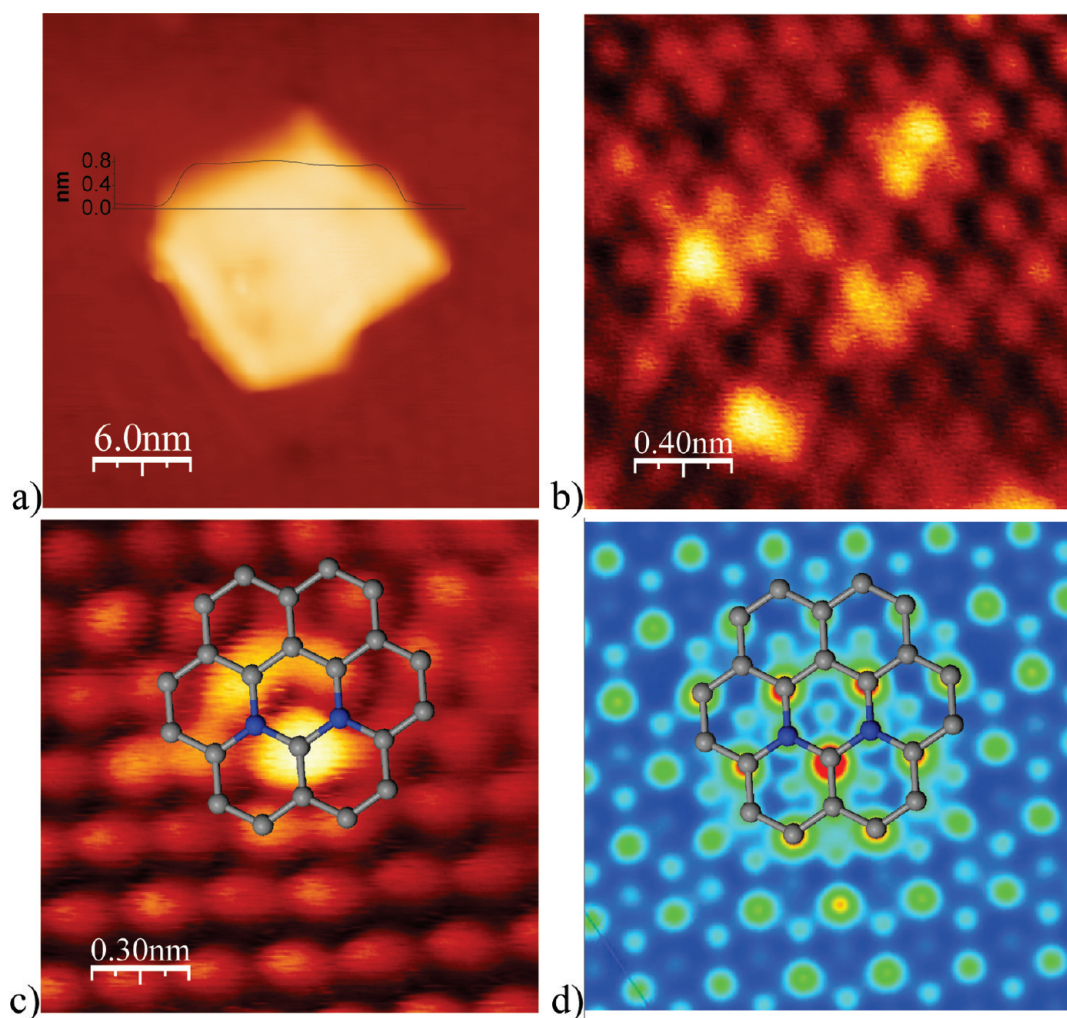
Figure 4. STM images of NG-2. (a) Isolated bilayer N-doped graphene and the black curve on top showing the height measurement across this bilayer.(b,c) High resolution images with defects arranged in different configurations, measured at a Bias = 0.5 V, current I = 53.4 pA, and Bias = 0.9 V, I = 104 pA, respectively. (d) Simulated STM image for (c). The inserted schematic structures represent N-doping graphene, with the hexagons in gray balls highlighting the atomic network of graphene and deep blue balls labeling N atoms.

The above results demonstrate that N-doped graphene has been successfully synthesized via a simple reaction between CCl_4 and Li_3N under mild conditions. Wang et al. previously synthesized CNTs on the basis of a reaction between CCl_4 and K in benzene, where free C=C was proposed to be the intermediate.[40]

Therefore, we propose that dichlorocarbene, free $-C=C-$, and $-C=N-$ groups are likely the intermediates during transformation of sp^3 hybridized carbon in CCl_4 to sp^2 hybridized carbon. These intermediates should readily couple with each other going through further dechlorination and forming small domains of

1191
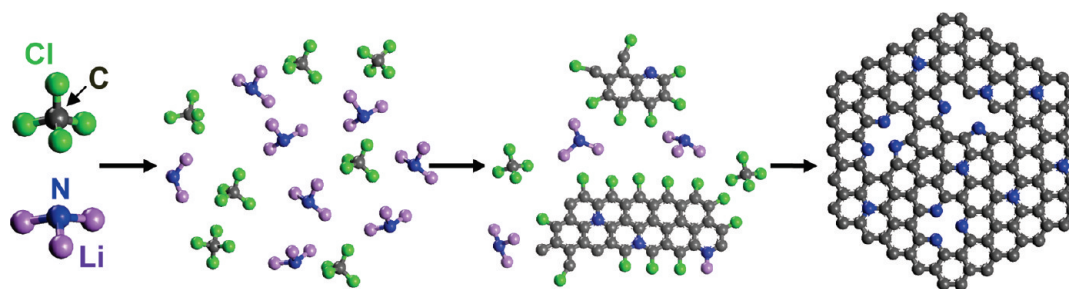
Figure 5. Scheme of a proposed mechanism for solvothermal synthesis of N-doped graphene via the reaction of CCl_4 and Li_3N, where gray balls represent C atoms, blue for N, green for Cl, and purple for Li.

sp^2 hybridized carbon containing N and then grow into N-doped graphene sheets. Figure 5 illustrates the proposed mechanism.

This free-standing N-doped graphene can be interesting as a metal-free catalyst because of its high electron conductivity and high content of nitrogen. N-doped CNTs from pyrolysis of iron(II) phthalocyanine[19] and CVD-derived N-graphene[41] have been found to facilitate the fuel cell cathode oxygen reduction reaction (ORR) earlier. In order to understand if the incorporation of N atoms in the graphene structure is sufficient to activate oxygen, we carried out DFT calculation (Figure S5 of the Supporting Information). The results show that oxygen can be activated in the presence of both graphitic and pyridinic N species. For graphitic N, because of the higher electronegativity of N than C, electrons transfer from the adjacent C to N atoms, and N backdonates electrons to adjacent C p_z orbitals. The donation and backdonation process does not only facilitate O_2 dissociation on the adjacent C atoms but also helps form a strong chemical bond between O and C. For pyridinic N located at the graphene edge, oxygen can be activated via direct bonding with the lone pair electrons of N. The dissociative adsorption energies of oxygen are similar on both graphitic and pyridinic N-doped graphene (Figure S5 of the Supporting Information). Therefore, one can enhance the activity by creating more active sites through increasing the nitrogen content. We tested the N-doped graphene materials as electrocatalysts for ORR. Indeed, our preliminary results show that they are more active than pure graphene and commercial XC-72 (Figure S6 of the Supporting Information) due to N incorporation. As expected, NG-2 exhibits a higher activity than NG-1 because the former contains more N species.

CONCLUSIONS

N-doped graphene has been synthesized by a one-step solvothermal method through the reaction of tetrachloromethane and lithium nitride. A gram scale is easily obtained in the laboratory, and this method allows scalable synthesis. Characterization results suggest that nitrogen species have been incorporated into the graphene structure with content in the range of 4.5−16.4%. The detailed defect structures have been investigated for the first time by STM, which reveals perturbed electronic structure due to N doping. This effect of nitrogen doping on the structure of graphene is further confirmed by DFT simulation. The resulting N-doped graphene is anticipated to find applications as a metal-free material for catalytic reactions involving oxygen activation and as a solid base catalyst.[18] It can also promote further development of graphene for applications in other fields such as electronics, supercapacitors, and lithium batteries.

ASSOCIATED CONTENT

ⓢ **Supporting Information.** TEM images of NG-1; wide XPS spectra of NG-1 and NG-2 and N1s XPS spectra of NG-2 upon in situ heat treatment; atomic model for N-doped graphene; elemental compositions of NG-1 and NG-2; STM image of the SiC (0001) substrate; DFT calculation of oxygen activation by N-doped graphene; oxygen reduction voltammogram of pure graphene, XC-72, NG-1-600, NG-2-600, and 40% Pt-C/GC. This material is available free of charge via the Internet at http://pubs.acs.org.

AUTHOR INFORMATION

Corresponding Author
*E-mail: panxl@dicp.ac.cn (X.P.); xhbao@dicp.ac.cn (X.B.).

ACKNOWLEDGMENT

REFERENCES

(1) Geim, A. K.; Novoselov, K. S. *Nat. Mater.* **2007**, *6*, 183–191.

(2) Zhang, K.; Zhang, L. L.; Zhao, X. S.; Wu, J. S. *Chem. Mater.* **2010**, *22*, 1392–1401.

(3) Allen, M. J.; Tung, V. C.; Kaner, R. B. *Chem. Rev.* **2010**, *110*, 132–145.

(4) Murugan, A. V.; Muraliganth, T.; Manthiram, A. *Chem. Mater.* **2009**, *21*, 5004–5006.

(5) Deifallah, M.; McMillan, P. F.; Cora, F. *J. Phys. Chem. C* **2008**, *112*, 5447–5453.

(6) Cervantes-Sodi, F.; Csanyi, G.; Piscanec, S.; Ferrari, A. C. *Phys. Rev. B* **2008**, *77*, 165427.

(7) Li, Y. F.; Zhou, Z.; Shen, P. W.; Chen, Z. F. *Acs Nano* **2009**, *3*, 1952–1958.

(8) Li, X. L.; Wang, H. L.; Robinson, J. T.; Sanchez, H.; Diankov, G.; Dai, H. J. *J. Am. Chem. Soc.* **2009**, *131*, 15939–15944.

(9) Lin, Y. C.; Lin, C. Y.; Chiu, P. W. *Appl. Phys. Lett.* **2010**, *96*, 133110.

(10) Wei, D. C.; Liu, Y. Q.; Wang, Y.; Zhang, H. L.; Huang, L. P.; Yu, G. *Nano Lett.* **2009**, *9*, 1752–1758.

(11) Panchokarla, L. S.; Subrahmanyam, K. S.; Saha, S. K.; Govindaraj, A.; Krishnamurthy, H. R.; Waghmare, U. V.; Rao, C. N. R. *Adv. Mater.* **2009**, *21*, 4726–4730.

(12) Li, Y. D.; Qian, Y. T.; Liao, H. W.; Ding, Y.; Yang, L.; Xu, C. Y.; Li, F. Q.; Zhou, G. *Science* **1998**, *281*, 246–247.

(13) Jiang, Y.; Wu, Y.; Zhang, S. Y.; Xu, C. Y.; Yu, W. C.; Xie, Y.; Qian, Y. T. *J. Am. Chem. Soc.* **2000**, *122*, 12383–12384.

(14) Hu, G.; Ma, D.; Cheng, M.; Liu, L.; Bao, X. H. *Chem. Commun.* **2002**, 1948–1949.

(15) Choucair, M.; Thordarson, P.; Stride, J. A. *Nature Nanotechnol.* **2009**, *4*, 30–33.

(16) Chen, W.; Chen, S.; Qi, D. C.; Gao, X. Y.; Wee, A. T. S. *J. Am. Chem. Soc.* **2007**, *129*, 10418–10422.

(17) Tersoff, J.; Hamann, D. R. *Phys. Rev. Lett.* **1983**, *50*, 1998–2001.

(18) van Dommele, S.; de Jong, K. P.; Bitter, J. H. *Chem. Commun.* **2006**, 4859–4861.

(19) Gong, K. P.; Du, F.; Xia, Z. H.; Durstock, M.; Dai, L. M. *Science* **2009**, *323*, 760–764.

(20) Casanovas, J.; Ricart, J. M.; Rubio, J.; Illas, F.; JimenezMateos, J. M. *J. Am. Chem. Soc.* **1996**, *118*, 8071–8076.

(21) Maldonado, S.; Morin, S.; Stevenson, K. J. *Carbon* **2006**, *44*, 1429–1437.

(22) Malard, L. M.; Pimenta, M. A.; Dresselhaus, G.; Dresselhaus, M. S. *Phys. Rep.* **2009**, *473*, 51–87.

(23) Ferrari, A. C.; Meyer, J. C.; Scardaci, V.; Casiraghi, C.; Lazzeri, M.; Mauri, F.; Piscanec, S.; Jiang, D.; Novoselov, K. S.; Roth, S.; Geim, A. K. *Phys. Rev. Lett.* **2006**, *97*, 187401.

(24) Deng, D. H.; Pan, X. L.; Zhang, H.; Fu, Q.; Tan, D. L.; Bao, X. H. *Adv. Mater.* **2010**, *22*, 2168–2171.

(25) Lee, Y. T.; Kim, N. S.; Bae, S. Y.; Park, J.; Yu, S. C.; Ryu, H.; Lee, H. J. *J. Phys. Chem. B* **2003**, *107*, 12958–12963.

(26) Kang, H. S.; Jeong, S. *Phys. Rev. B* **2004**, *70*, 233411.

(27) Cruz-Silva, E.; Lopez-Urias, F.; Munoz-Sandoval, E.; Sumpter, B. G.; Terrones, H.; Charlier, J. C.; Meunier, V.; Terrones, M. *Acs Nano* **2009**, *3*, 1913–1921.

(28) Ewels, C. P.; Glerup, M. *J. Nanosci. Nanotech.* **2005**, *5*, 1345–1363.

(29) Dresselhaus, M. S.; Dresselhaus, G.; Saito, R.; Jorio, A. *Phys. Rep.* **2005**, *409*, 47–99.

(30) Dresselhaus, M. S.; Dresselhaus, G. *Adv. Phys.* **2002**, *51*, 1–186.

(31) Jiao, L. Y.; Zhang, L.; Wang, X. R.; Diankov, G.; Dai, H. J. *Nature* **2009**, *458*, 877–880.

(32) Gao, L. B.; Ren, W. C.; Liu, B. L.; Saito, R.; Wu, Z. S.; Li, S. S.; Jiang, C. B.; Li, F.; Cheng, H. M. *Acs Nano* **2009**, *3*, 933–939.

(33) Zheng, B.; Hermet, P.; Henrard, L. *Acs Nano* **2010**, DOI: 10.1021/nn1002425.

(34) Lauffer, P.; Emtsev, K. V.; Graupner, R.; Seyller, T.; Ley, L.; Reshanov, S. A.; Weber, H. B. *Phys. Rev. B* **2008**, *77*, 155426.

(35) Brar, V. W.; Zhang, Y.; Yayon, Y.; Ohta, T.; McChesney, J. L.; Bostwick, A.; Rotenberg, E.; Horn, K.; Crommie, M. F. *Appl. Phys. Lett.* **2007**, *91*, 122102.

(36) Simon, L.; Bena, C.; Vonau, F.; Aubel, D.; Nasrallah, H.; Habar, M.; Peruchetti, J. C. *Eur. Phys. J. B* **2009**, *69*, 351–355.

(37) Rutter, G. M.; Crain, J. N.; Guisinger, N. P.; Li, T.; First, P. N.; Stroscio, J. A. *Science* **2007**, *317*, 219–222.

(38) Amara, H.; Latil, S.; Meunier, V.; Lambin, P.; Charlier, J. C. *Phys. Rev. B* **2007**, *76*, 115423.

(39) Paredes, J. I.; Villar-Rodil, S.; Solis-Fernandez, P.; Martinez-Alonso, A.; Tascon, J. M. D. *Langmuir* **2009**, *25*, 5957–5968.

(40) Wang, X. J.; Lu, J.; Xie, Y.; Du, G.; Guo, Q. X.; Zhang, S. Y. *J. Phys. Chem. B* **2002**, *106*, 933–937.

(41) Qu, L. T.; Liu, Y.; Baek, J.-B.; Dai, L. M. *Acs Nano* **2010**, *4*, 1321–1326.